




## Article

# Relative Sea-Level Changes During the Upper Holocene as Determined by Reference to Beachrock Formations Along the South Coastline of Cyprus and Their Correlation with the Archaeological Context of the Island

Miltiadis Polidorou <sup>1,\*</sup>, Giannis Saitis <sup>2</sup>, Anna Karkani <sup>2</sup> and Judith Gatt <sup>3</sup>

<sup>1</sup> Digital Humanities GeoInformatics Lab, Archaeological Research Unit, Department of History and Archaeology, University of Cyprus, Nicosia 1678, Cyprus

<sup>2</sup> Department of Geology and Geoenvironment, School of Science, National and Kapodistrian University of Athens, 15784 Athens, Greece; saiti@geol.uoa.gr (G.S.); ekarkani@geol.uoa.gr (A.K.)

<sup>3</sup> Aix-Marseille Université, CNRS, Centre Camille Jullian, Aix-en-Provence, France and Department of History and Archaeology, University of Cyprus, Nicosia 1678, Cyprus; judith.gatt@univ-amu.fr

\* Correspondence: polidorou.miltiadis@ucy.ac.cy; Tel.: +357-99396863

**Abstract:** This study examines the relative sea-level changes during the Upper Holocene period along the south coastline of Cyprus through the investigation of beachrock formations and their impact on archaeological sites. Beachrock, as a natural indicator of past relative sea levels, provides valuable insights into the dynamic interplay between sea-level fluctuations and human settlements. The research integrates field observations, mineralogical and geochemical analysis, geochronological studies, and archaeological data to reconstruct past sea-level variations and their implications for coastal archaeological sites. The results reveal significant fluctuations in relative sea levels during the Upper Holocene, influencing the development and occupation of coastal archaeological sites. By elucidating the complex relationship between sea-level changes and human activity, this study contributes to our understanding of past coastal environments and their socio-cultural dynamics. Moreover, it underscores the importance of considering geological factors in archaeological interpretations and coastal management strategies in the face of contemporary sea-level rise.

**Keywords:** relative sea-level fluctuation; geomorphology; geoarchaeology; eastern Mediterranean; palaeogeographic reconstruction



Academic Editor: Fedor Lisetskii

Received: 15 February 2025

Revised: 21 March 2025

Accepted: 31 March 2025

Published: 4 April 2025

**Citation:** Polidorou, M.; Saitis, G.; Karkani, A.; Gatt, J. Relative Sea-Level Changes During the Upper Holocene as Determined by Reference to Beachrock Formations Along the South Coastline of Cyprus and Their Correlation with the Archaeological Context of the Island. *Geosciences* **2025**, *15*, 137. <https://doi.org/10.3390/geosciences15040137>

**Copyright:** © 2025 by the authors. Licensee MDPI, Basel, Switzerland. This article is an open access article distributed under the terms and conditions of the Creative Commons Attribution (CC BY) license (<https://creativecommons.org/licenses/by/4.0/>).

## 1. Introduction

Beachrock formation and relative sea-level change are two interlinked geological and environmental processes that have played important roles in shaping coastal landscapes and understanding the Earth's dynamic history [1–3]. Beachrock, a distinctive geological formation, serves as a tangible record of the relationship between the sea and the land. The sea level, on the other hand, is a dynamic parameter that dictates the boundaries of coastlines and influences the formation and preservation of beachrock [4–7]. Together, these two phenomena provide insights into environmental changes and coastal changes, and the ongoing challenges posed by rising sea levels for human activities [8–11].

Throughout the Earth's history, sea levels have been subject to dynamic changes driven by a complex interplay of climatic, tectonic, and oceanographic factors [7,12–14]. In the eastern Mediterranean, these fluctuations have left their mark on coastal environments, profoundly influencing human civilisation, biodiversity, and geological processes [5,6,10,15].

Numerous studies have taken place in the Mediterranean studying relative sea-level changes [16–19]. Different relative sea level (RSL) estimates are derived from different areas of the Mediterranean owing mainly to the active tectonics of the eastern part. On the Tyrrhenian coasts of Italy, Evelpidou et al., (2012) [20] estimated that during the Roman period, the relative sea level was located between  $32 \pm 5$  cm and  $58 \pm 5$  lower than present, based on detailed research on fish tanks. On the coasts of Israel, Sivan et al., (2001) [21] estimated that the RSL was lower than  $-3$  to  $-4.5$  m at 6000 BP and remained below the present level until 2000–3000 BP, based on archaeological observations and model predictions. Conversely, evidence from the coastal zone of Greece is characterised by different rates and modes due to the active tectonic regime. In the central Cyclades, Karkani et al., (2019) [19] estimated an RSL that rose by about 2 m in the last 2000 years and by more than 3.9 m since about 4500 years BP. On the other hand, Crete is characterised by blocks with variable vertical displacements [22].

As global climate change accelerates, understanding and quantifying the region's past sea level dynamics becomes increasingly vital for anticipating future coastal vulnerabilities and devising effective mitigation strategies [23–25]. Amongst the various coastal features that testify to past sea-level changes, beachrock can be very useful in quantifying RSL changes and coastal evolution. Beachrock has been extensively studied from around the world, and its formation, texture, and geometry have enabled numerous hypotheses about Holocene-relative or eustatic sea-level fluctuations [1,2,5,6,11,26,27]. Their basic characteristics like lithology and mineralogy [1,2,4,11,27] make them useful as robust sea-level index points (SLIPs) in the Mediterranean, in locations with tidal ranges less than 1 m [6,11,28,29]. The complex mineralogical, chemical, and lithological composition of beachrock offers a unique and valuable dataset to unravel the history of sea-level fluctuations in this region.

In this paper, we examine the formation, composition, and geochemical signatures of these coastal features, to reconstruct a comprehensive chronicle of RSL changes over the middle and upper Holocene along the south coast of Cyprus. Through this investigation, we endeavour to shed light on the coastline changes caused by relative sea-level fluctuations, and their influence on human activities in the coastal zone.

This study resonates with broader archaeological research issues as a more profound understanding of past sea-level variability provides a stable basis for the study of archaeological coastal remains in relation to the paleoshoreline, sustainable coastal management, safeguarding cultural heritage, and protecting the vulnerable ecosystems that line the shores of the eastern Mediterranean.

## 2. Study Area and Regional Tectonic Framework

The prominent geomorphic features of the island of Cyprus are mountainous areas to the north and south, a central plain, and several scattered alluvial coastal plains along the southern coast (Figure 1). Marine terraces are widely developed from 2 m to 360 m above mean sea level (a.m.s.l.) in southern Cyprus [30]. According to the long-term temperature and precipitation data, Cyprus has the typical Mediterranean climate regime characterised by average air temperatures of  $19.9$  °C to  $19.3$  °C, and average precipitation ranging between 481 mm and 310 mm, respectively [30]. Based on Danezis et al. (2020) [24], the tidal range is between 0.26 and 0.30 m, which is classified as a micro-tidal range.

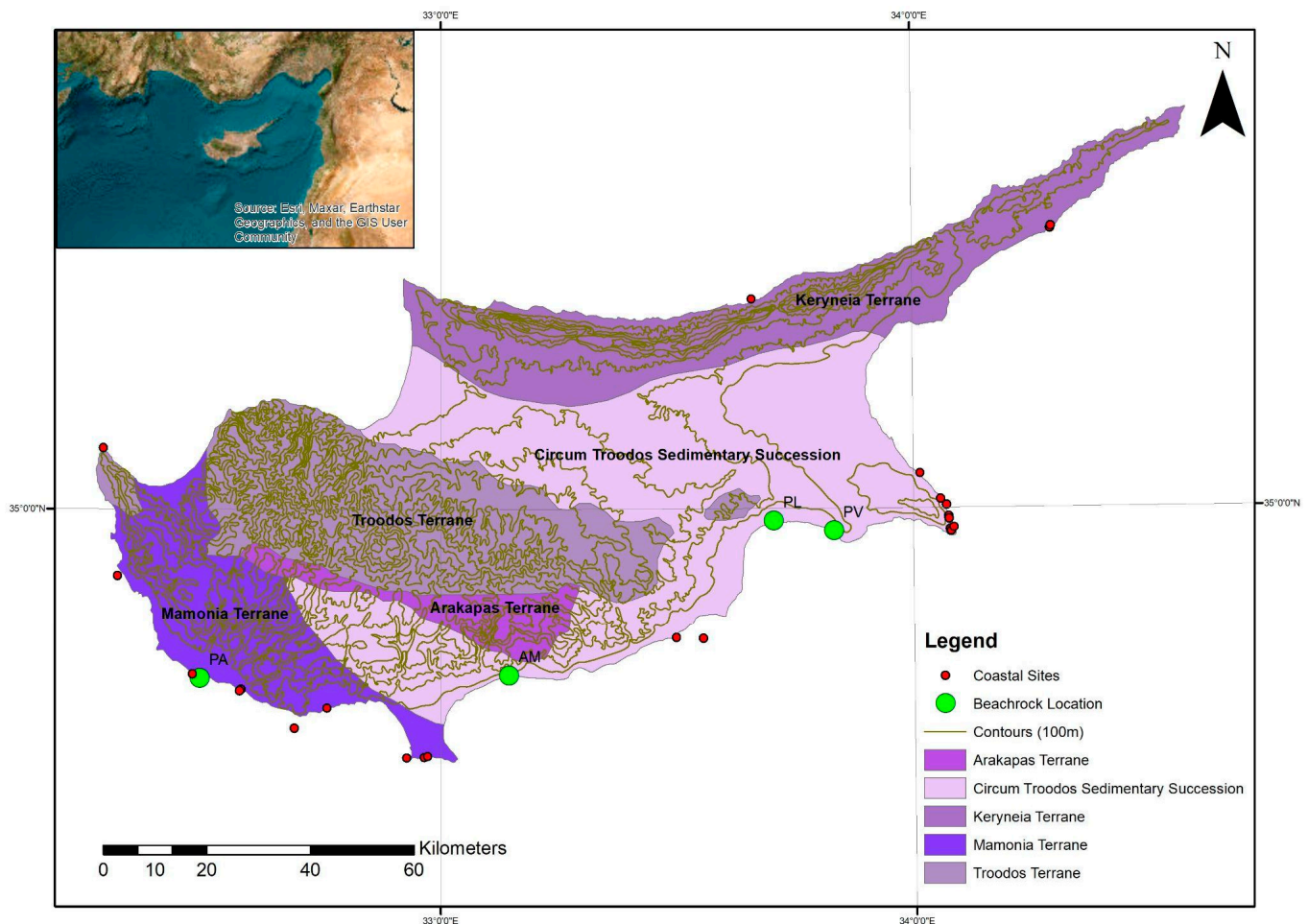


**Figure 1.** Geological zones of the study area and location of the beachrock (green symbol). Red symbols represent the coastal and near-shore underwater archaeological sites at the south coast of Cyprus.

Long-term tectonic uplift focused on the Troodos Mountain was the dominant control of geomorphology and fluvial deposition [30]. However, shorter-term climatic changes (on Milankovitch timescales) also played a key role [31,32]. Similar climatic influence is inferred for many other areas undergoing tectonic uplift, including Calabria [33] and south-central Australia [34]. Eustatic sea-level oscillations of up to c. 130 m took place during the Last Glacial Maximum (19,000 and 30,000 years ago) [35].

During the Holocene, the tectonic evolution of Cyprus was primarily influenced by the interactions of the African, Eurasian, and Arabian plates. A significant factor in this evolution was the westward escape of the Anatolian microplate, which was driven by the northward subduction of the Hellenic Arc and the resulting asthenospheric flow in the Aegean region [36]. The motion of Anatolia was accommodated by deformation along the major fault systems, such as the East Anatolian, North Anatolian, and Dead Sea Transform faults, which intersect near Cyprus [37,38]. The Dead Sea Transform and East Anatolian faults exhibit left-lateral strike-slip motion, while the North Anatolian fault is characterised by right-lateral strike-slip movement [39,40]. These fault systems have shaped the region over time, and the Latakia Ridge, in particular, transitioned from a compressional to a strike-slip regime during the late Miocene to Holocene, driven by the changes in regional tectonic stresses [41,42].

In addition, the early Pliocene collision of the African plate with the Cyprus Arc initiated subduction beneath the arc, contributing to the uplift of Cyprus [38,43]. This tectonic interaction continued into the Holocene, with the African plate moving north-northwest

and the Anatolian plate undergoing counterclockwise rotation [44,45]. These movements facilitated left-lateral strike-slip motion along the Latakia Ridge, further influencing the region's tectonic dynamics [46]. The cumulative effects of these tectonic forces, including faulting and seismic activity, have been crucial in the geological shaping of Cyprus, contributing to both the island's uplift and its seismic characteristics during the Holocene period [40,41].

### 3. Archaeological Context

The southern coast of Cyprus preserves several coastal archaeological and historical sites dating from the Epipalaeolithic period to the Ottoman period (Figure 1). Different types of sites are preserved, such as harbour structures, anchorages, coastal settlements, tombs, fortifications, quarries, and individual finds, some submerged or semi-submerged, while others are on the shoreline or along the coast a distance of a few metres from the sea.

These archaeological sites contribute to reconstructing the maritime history of the island while testifying to the diachronic changes in the coastline. The earliest human presence on the island is attested in the south-central coast of Cyprus, in the site, Akrotiri Aetokremnos, dating to the Epipalaeolithic period (11,000–9000 BCE, 12,950–10,950 BP) [47,48]. From the Initial Aceramic Neolithic to the Late Chalcolithic (9000–2400 BCE, 10,950–4350 BP), habitation on the coast was scarce (i.e., Kissonerga Mylouthkia, Maa Palaioakastro) [49]. In the Bronze Age (2450–1100 BCE, 4400–3050 BP) though, especially in the Middle and Late Bronze Age, an intense habitation of the coastline driven by the need to secure the export of copper is attested to through coastal sites located not far from copper resources (i.e., Enkomi, Hala Sultan Tekke) [50]. These settlements prepared the ground for the Iron Age (1100–450 BCE, 3050–2400 BP) Cypriot polities [51,52] which were also mainly located along the coast. In the Classical period (450–310 BCE, 2400–2260 BP), the Cypriot polities continued to occupy most of the coastline leading to an intense occupation and alteration of the coastscape with the construction of the earliest known harbours of the island [53]. In the Hellenistic period (310–30 BCE, 2260–1980 BP), the arrival of Ptolemy on the island led to the abolishment of the Cypriot polities [54]. Most of these centres of power, however, continued to be inhabited until the Byzantine period. During these times, especially in the Roman (30 BCE–284 CE, 1980–1666 BP) and Byzantine periods (284–1191 CE, 1666–759 BP), several small sites spread along the coastline and are attested to today through harbour structures, wells, quarries, anchorages, and other remains (i.e., Akrotiri-Dreamer's Bay, Kioni, Amathous, Avdimou) [55,56]. The habitation of the coast decreased significantly with the Arab raids (around the 7th century AD–1250 BP) but never ceased [57] as remains from Medieval (1191–1571 CE, 759–379 BP) and Ottoman times (1571–1878 CE, 379–72 BP) (i.e., the Larnaca and Nea Paphos castle) up until the 19th and 20th centuries (i.e., harbour structures built by the British) are still visible today.

The archaeological documentation and study of coastal sites in Cyprus have been ongoing since the 1930s with the first documentation of the harbour of Karpasia-Ayios Philon being produced by Joan du Plat Taylor [58]. Several surveys along the coastline mapped underwater and coastal remains throughout the years [58,59]. However, despite these efforts, the geoarchaeological study of these sites has been systematically applied in only two coastal sites, Hala Sultan Tekke [9] and Kition [10,60]. However, only in Kition's naval harbour basin have relative sea-level-change estimations been based on cores and the detailed documentation of the shipsheds, providing a relative sea level for the Classical period of +0.80 m ( $\pm 0.20$  m) [60]. The lack of detailed measurements and geoarchaeological studies in the majority of the coastal archaeological sites leaves pending questions regarding the location of the paleo coastline, the change in the RSL in the long durée and its impact on the preservation and localisation of archaeological sites.



## 4. Methodology

### 4.1. Fieldwork and Laboratory

Beachrock was mapped in detail with a differential global positioning system (DGPS) and global navigation satellite system (GNSS) system receiver (Spectra SP60, Spectra Geospatial, Westminster, CO, USA, JGC, Marousi Attica, Greece). At each site, beachrock characteristics were recorded in detail, i.e., elevation/depth (in relation to the mean sea level), length, and width, with an accuracy of 3 cm. One or more transects were accomplished at each site, which also included sampling of the beachrock slabs (Figure 2).



**Figure 2.** Characteristic photos of beachrock from the study areas (a) Pafos airport beachrock, (b) Amathous beachrock, (c) Pyla beachrock, and (d) Xylophagou beachrock.

Beachrock samples were collected from the top bed for microscopic analysis. Eight thin sections were prepared for petrographic and microstratigraphic analysis aiming to determine the constituents, the presence of bioclasts, and the cement types. Beachrock samples were retrieved from the most seaward and landward parts of each slab as they are considered the most representative. The thin sections were examined through the use of a Leica DMLP (Leica Microsystems GmbH, Wetzlar, Germany) petrographic microscope with a digital camera and the corresponding image treatment software.

The bulk mineralogy of the samples was determined via X-ray diffraction (XRD), using a Panalytical X'pert- Pro X-Ray diffractometer with a Cu X-ray tube ( $K\alpha$  of Cu,  $\lambda = 1.5405 \text{ \AA}$ ), graphite monochromator, an applied voltage of 30 kV, and a 40 mA current.

The random powder mounts of samples, prepared via back loading, were scanned from  $2^{\circ}$  to  $70^{\circ}$   $2\theta$ . Powder diffraction data were collected at room temperature, and evaluated using the XPert High-Score (Version 2004) (PANalytical B.V., Almelo, The Netherlands), EVA software V6 provided by Bruker (Bruker AXS GmbH, Karlsruhe, Germany) and DIFFRACplus EVA v12.0. and managed using the PDF-2 database (International Centre for Diffraction Data, Newtown Square, PA, USA).

#### 4.2. Luminescence Dating

The beachrock was dated by using the optically stimulated luminescence (OSL) dating of quartz. Seven samples in total were collected, packed, and shipped according to the Luminescence Dating Laboratory instructions. The samples were processed at the Luminescence Dating Laboratory of the Institute of Physics, Silesian University of Technology, Poland. Quartz grains of 125–200  $\mu\text{m}$  size were selected for use. A germanium spectrometer was used to determine the radioactivity dose rate. The determination of the equivalent dose was measured using the single aliquot regeneration protocol (OSL-SAR) [61].

#### 4.3. Reconstruction of the Relative Sea Level

The beachrock data collected were used to reconstruct the RSL changes in our study area, through the production of Sea-Level Index Points (SLIPs) [62–64]. This methodology has been used in several recent Mediterranean studies [11,16,19,26,65]. For the dated samples, SLIPs are calculated based on the following equation:

$$\text{SLIP}_n = A_n - \text{RWL}_n$$

where  $A_n$  is the altitude of the indicator (beachrock), and  $\text{RWL}_n$  is the reference water level for that marker. The vertical errors for each SLIP included the indicative range and an error of  $\pm 0.03$  m for the samples' altitude [62].

SLIPs were produced for the beachrock samples that indicate a clear intertidal formation, based on their cement characteristics [29].

## 5. Results

### 5.1. Beachrock Distribution

Detailed spatial mapping of the exposed beachrock of South Cyprus was performed during the summers of 2021 and 2022. The analysis included the beachrock of the areas: Paphos Airport (PA), Amathous (AM), Pyla (PL), and Xylophagou (PV) (Figure 1).

The beachrock located near Paphos airport is composed of thin (3–5 cm thickness) pile layers of sediments with a plane-parallel seaward dip. The beachrock is quite extensive without signs of alterations such as broken parts and/or any gravitational signs or any vertical erosional features. The beachrock is located under a footwall of local calcareous sandstone. The exposed slab of the beachrock is 30 m long, mainly parallel to the base level and situated between +0.5 and  $-0.5$  m to the mean sea level (Figure 3).

The Amathous beachrock presents a special case as it is located in the middle of the submerged port of Amathous [66]. The beachrock is characterised by a thick sediment composition with an almost plane-parallel seaward dip of around  $2^{\circ}$ . The beachrock outcrop is submerged  $-1$  m deep and has a short width of 2.5 m and height of 10 cm (Figure 4).

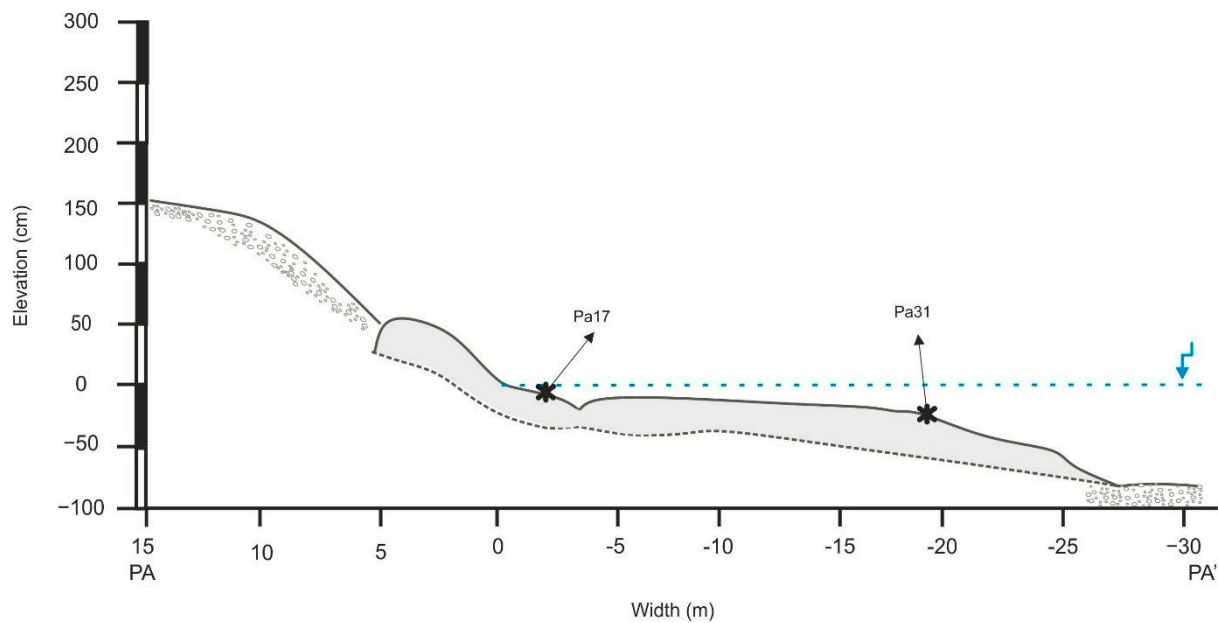


**Figure 3.** Representation of beach and beachrock profiles for Paphos Airport site. Blue line indicates the local m.s.l. Samples used for OSL dating and microscopic analysis are indicated by the star symbol.

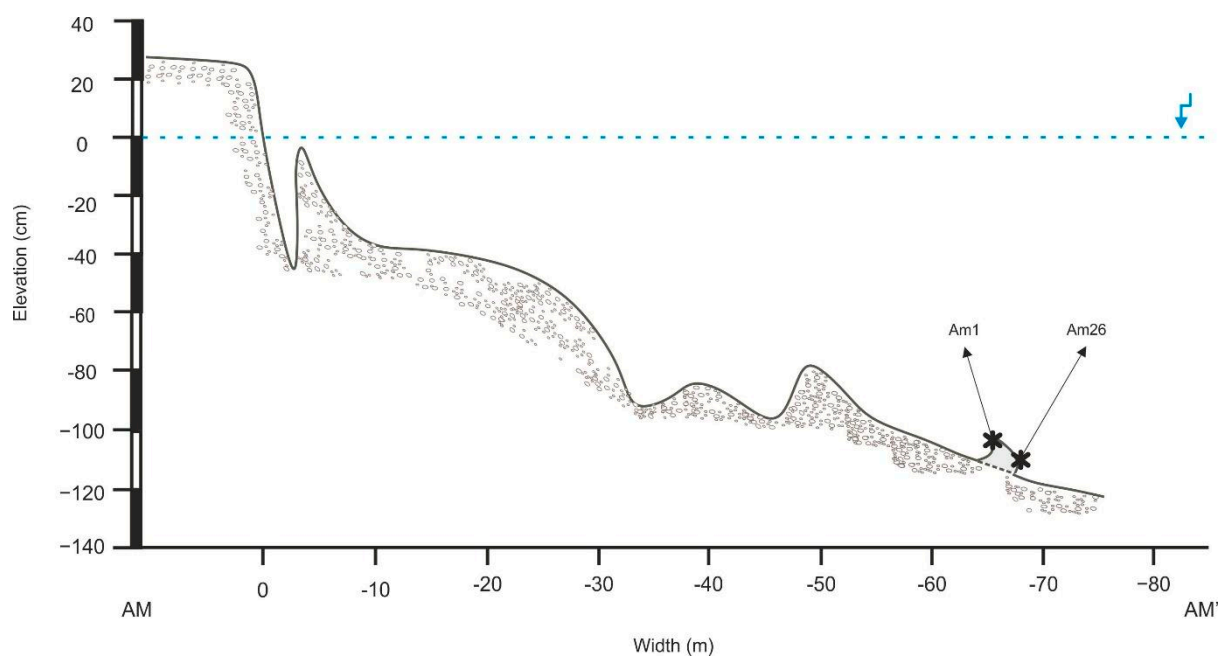


**Figure 4.** Representation of beach and beachrock profiles for Amathous site. Blue line indicates the local m.s.l. Samples used for OSL dating and microscopic analysis are indicated by the star symbol.

The Pyla beachrock consists of fine-grained sand with a thick plane-parallel seaward dip of  $5^\circ$ . The beachrock is situated approximately 10 m from the current coastline with a temporal tombolo formed at its landward part. The beachrock outcrop has a length of 72 m and width of 10 m, and lies between +0.3 and  $-1$  m to the mean sea level (Figure 5).

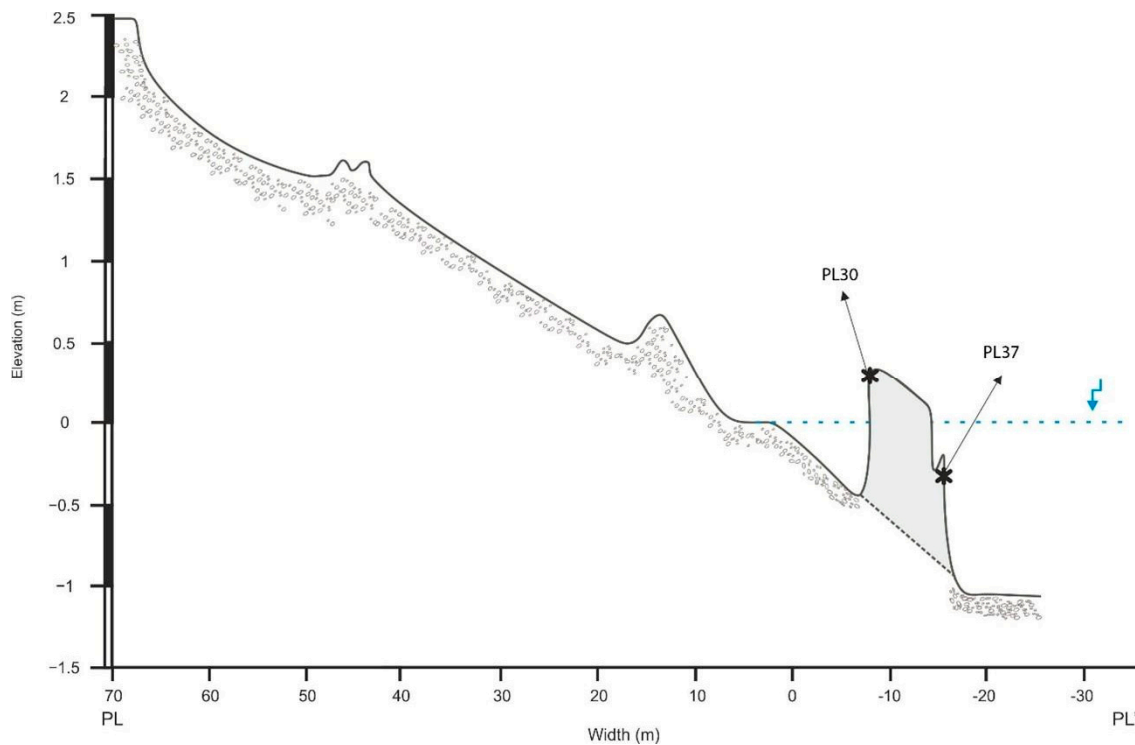


**Figure 5.** Representation of beach and beachrock profiles for Pyla site. Blue line indicates the local m.s.l. Samples used for OSL dating and microscopic analysis are indicated by the star symbol.

The final studied beachrock is located at Xylophagou. The beachrock slab is extensive and well formed with a seaward dip of  $8^\circ$ . The beachrock slab is observed covering a pocket beach having a length of 57 m and a width of 13 m, and is situated between +0.42 m and  $-0.45$  m to the mean sea level (Figure 6).

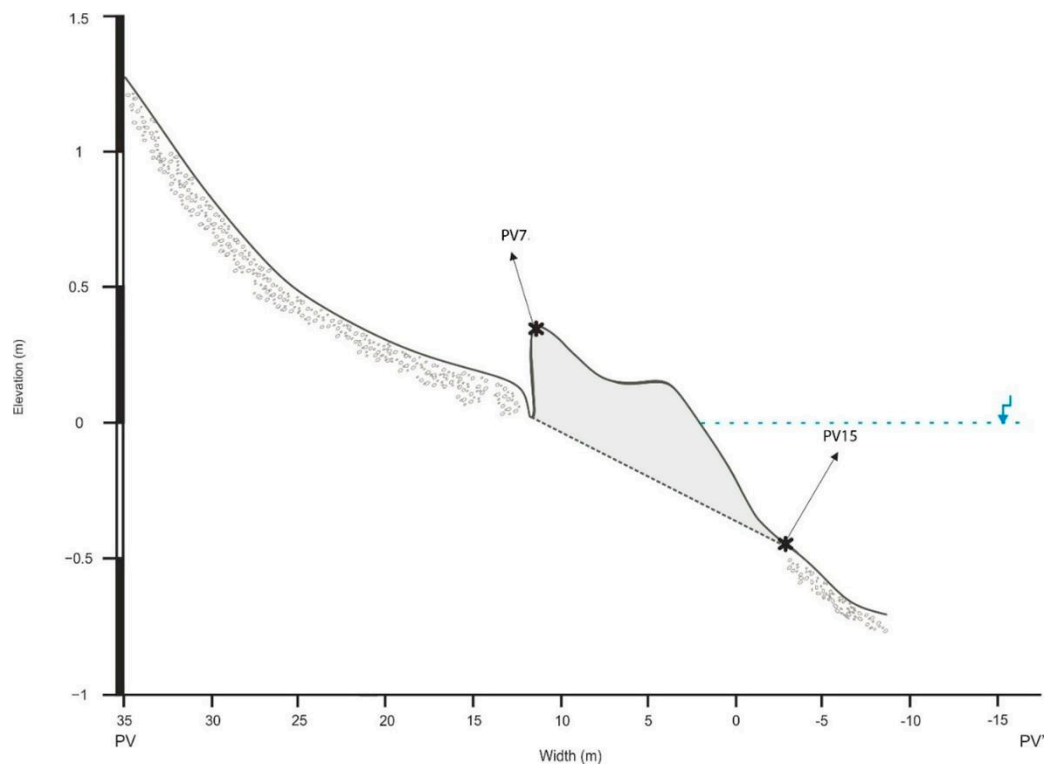


**Figure 6.** Representation of beach and beachrock profiles for Xylophagou site. Blue line indicates the local m.s.l. Samples used for OSL dating and microscopic analysis are indicated by the star symbol.



### 5.2. Cement Morphology

All the observed beachrock samples show a coherent pattern with sub-rounded and well to medium sorted grains with a limited bioclasts presence (<10%). The examination of the beachrock cements from Paphos airport, Amathous, Pyla, and Xylophagou showed that the micritic High Magnesium Calcite (HMC) [(Ca,Mg)CO<sub>3</sub>] cement was the most dominant in all the samples (Table 1). The Paphos airport beachrock consists mainly of lithoclasts as bioclasts are absent. Both samples PA17 and PA31 are characterised by thin micritic (<10 µm) cement forming an isopachous coating around the sediment grains (Figure 7). The seaward sample, PABrS31, is composed of bladed cements while matrix and pore-filling cements were observed consisting of very fine sedimentary particles (5–20 µm) resulting in a coherent coating. Furthermore, the PA31 sample has brown micritic cement forming an outer film.

**Table 1.** XRD results.

Sample	Cement Type
PA17	Quartz, Calcium Carbonate, Hornblende, Albite, Clinocllore, Clinopyroxene, Clinochrysotile
PA31	Quartz, Calcium Carbonate, Manganocalcite, Albite, Clinocllore, Clinopyroxene
AM26	Quartz, Calcium Carbonate, Magnesiohornblende, Albite, Clinocllore, Clinopyroxene, Dolomite
PL30	Quartz, Calcium Carbonate, Magnesiohornblende, Albite, Clinocllore, Clinopyroxene, Aragonite
PV7	Quartz, Calcium Carbonate, Magnesiohornblende, Albite, Clinocllore, Clinopyroxene
PV15	Quartz, Calcium Carbonate, Magnesiohornblende, Albite, Clinocllore, Clinopyroxene, Epidote, Montmorillonite

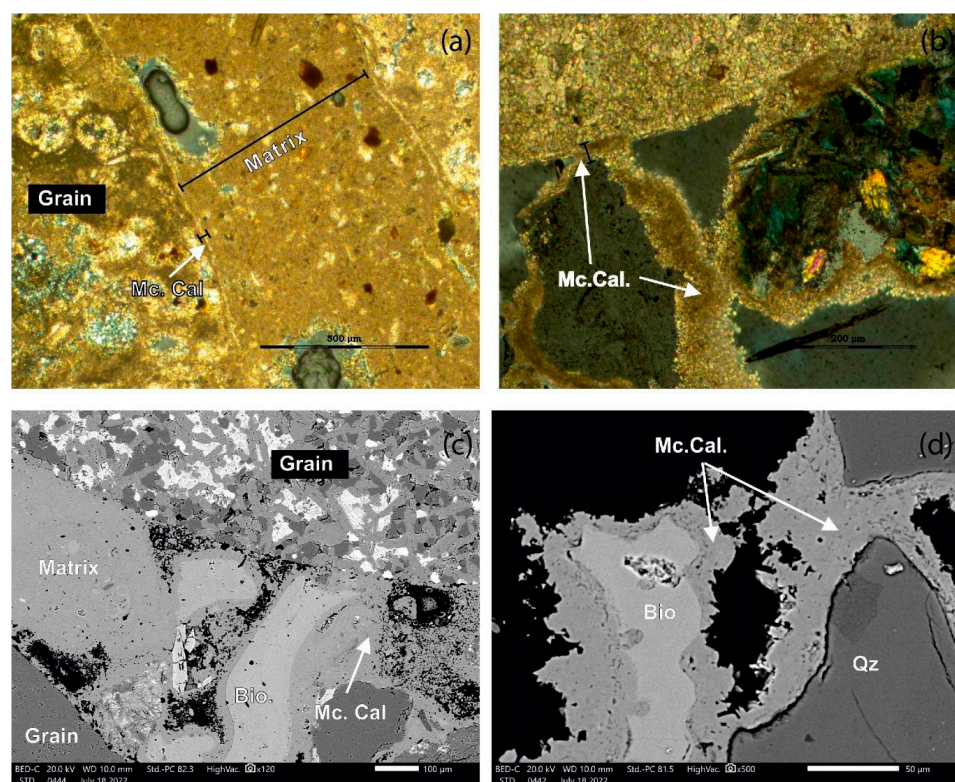


**Figure 7.** Paphos airport sample analysis; abbreviations: Mc.Cal., micritic High Magnesium Calcite, Bio., biogenic calcite/shells. Polarised microscopy images (a) sample PA17, 20× magnification, scale 200 µm. Micritic HMC cement is coating mineral and lithoclast grains. (b) Sample PA31, 10× magnification, scale 500 µm. Thin micritic HMC cement is coating lithoclast grains while filling pores and micro particles as matrix. SEM images (c) sample PA17, scale 50 µm. The micritic HMC cement is covering the grains as a pore-filling HMC cement. (d) Sample PA31, scale 100 µm. Micritic HMC cement is covering the sediment lithoclast, and biological grains, pore-filling HMC cement, and matrix are observed.

The Amathous beachrock consists mainly of lithoclasts. The sample, AM1, is characterised by micritic ( $<20\text{ }\mu\text{m}$ ) cement forming acicular cement (Figure 8). The observed cement homogenously covers the pores while forming a thin outer brown-coloured film on sediments. The sample, AM26, is characterised by thick micritic cement ( $50\text{--}100\text{ }\mu\text{m}$ ) around lithoclast and bioclast grains as well as forming an isopachous coating around the sediment grains. Pore-filling cements were also observed resulting in a coherent cementation.

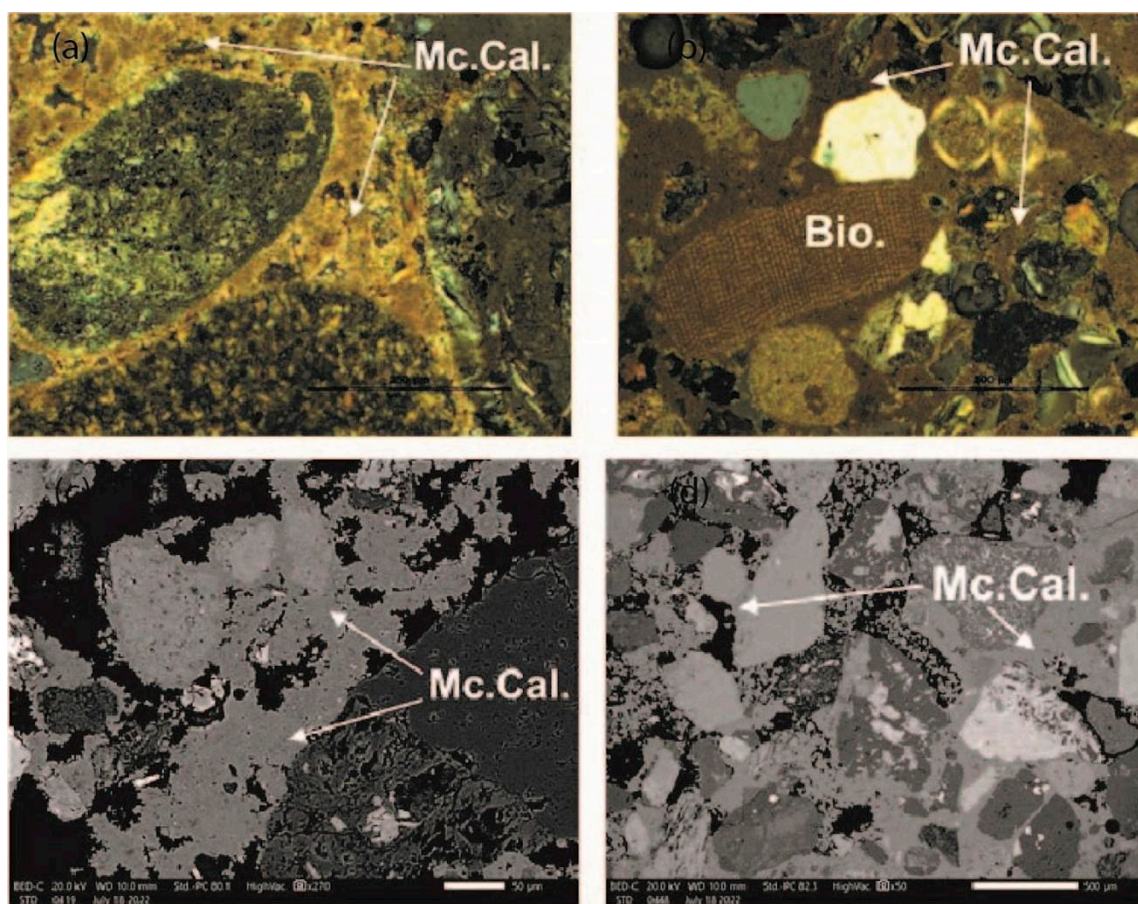


**Figure 8.** Amathous sample analysis; abbreviations: Mc.Cal., micritic High Magnesium Calcite, Bio., biogenic calcite/shells. Polarised microscopy images (a) sample AM1, 20× magnification, scale 250  $\mu\text{m}$ . Micritic HMC cement is coating mineral and lithoclast grains. (b) Sample AM26, 10× magnification, scale 500  $\mu\text{m}$ . Thin micritic HMC cement is coating lithoclast and bioclasts grains while filling pores. SEM images (c) sample AM1, scale 50  $\mu\text{m}$ . The micritic HMC cement covers the grains as a pore-filling cement. (d) Sample AM26, scale 500  $\mu\text{m}$ . Micritic HMC cement covers the sediment lithoclast, and pore-filling HMC cement and meniscus are observed.

The Pyla beachrock samples consist mainly of lithoclasts as bioclasts are absent. Both samples are characterised by thin micritic ( $10\text{--}20\text{ }\mu\text{m}$ ) cement forming a bladed isopachous coating around the sediment grains (Figure 9). The cement is observed to homogenously fill the pores while sample PL30 formed a thin outer brown-coloured film on sediments. The seaward sample PL37 is observed with matrix formation consisting of very fine sedimentary particles and cemental concentrations forming pellets. The pore-filling cements resulted in a coherent cementation.



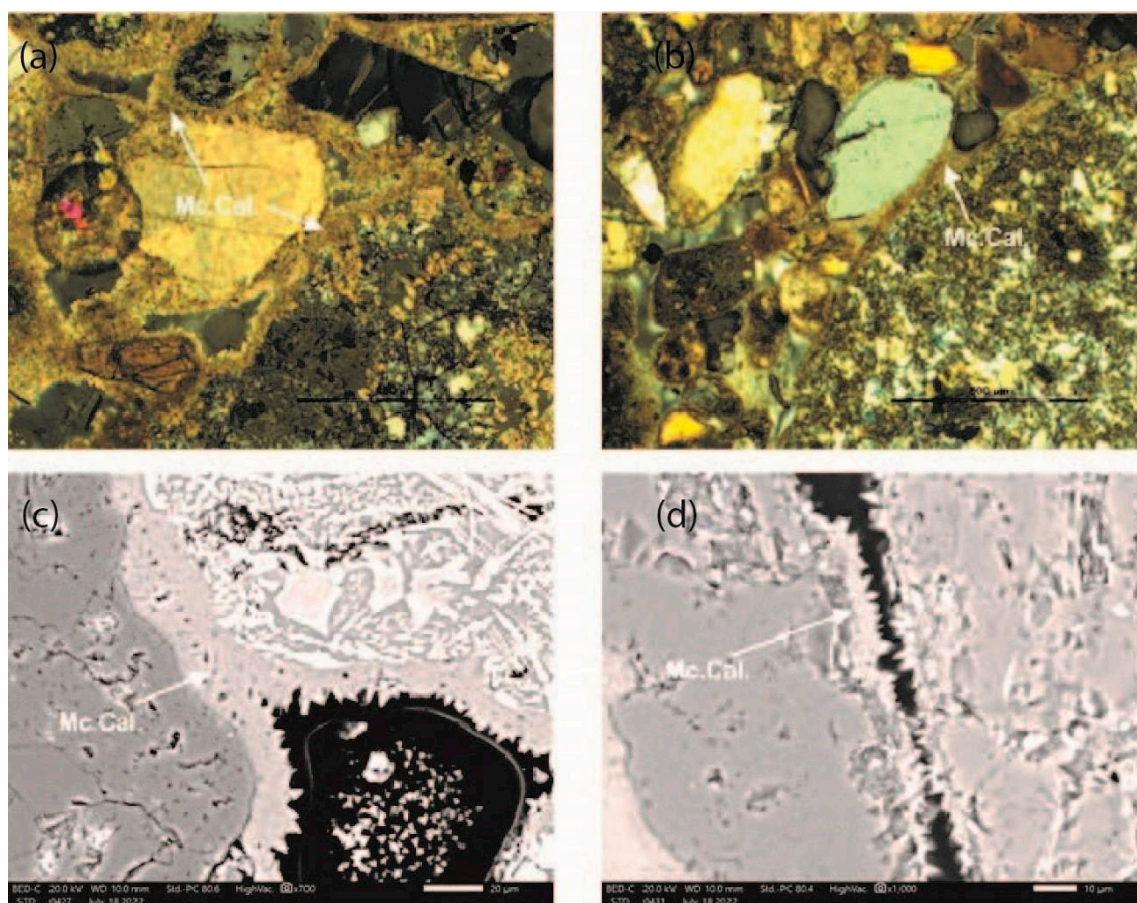


**Figure 9.** Pyla sample analysis; abbreviations: Mc.Cal., micritic High Magnesium Calcite. Polarised microscopy images (a) sample PL30, 20× magnification, scale 250 µm. Micritic HMC isopachous cement is coating mineral and lithoclast grains. (b) Sample PL37, 10× magnification, scale 500 µm. Thin micritic HMC cement is coating minerals and lithoclast grains. SEM images (c) sample PL30, scale 20 µm. The micritic HMC cement is binding two sediment grains, and the bladed isopachous form is well observed. (d) Sample PL37, scale 10 µm. Thin micritic HMC cement is binding two sediment grains; the bladed isopachous form is well observed.

The Xylophagou beachrock samples consist of lithoclast and bioclast sediment grains. Both samples, PV7 and PV15, are characterised by a thin isopachous micritic (20 µm) cement formation coating the sediment grains (Figure 10). The cement is observed to homogeneously cover the pores, while in sample PV7, a thin outer brown-coloured biomicritic film formed on sediments as well as cemental concentrations forming pellets. The PV17 sample yielded additional sparitic cement and locally, the cement fringes reached 40 µm. The bioclasts cover nearly 20% of the sample surface. The pore-filling cements resulted in a coherent cementation.

The observed binding material between grains is mostly upper-middle intertidal cement in all the samples of the four study areas. The cements of the upper intertidal zone are associated with detrital constituents (rock and shell fragments) which are present in all the samples. Additionally, the presence of isopachous micritic coating cement crystals is another indication of the beachrock formation in the intertidal zone. The analysed samples also exhibited a lack of meteoric cement which usually consists of LMC cements with sparse micritic crystals forming a meniscus [29].

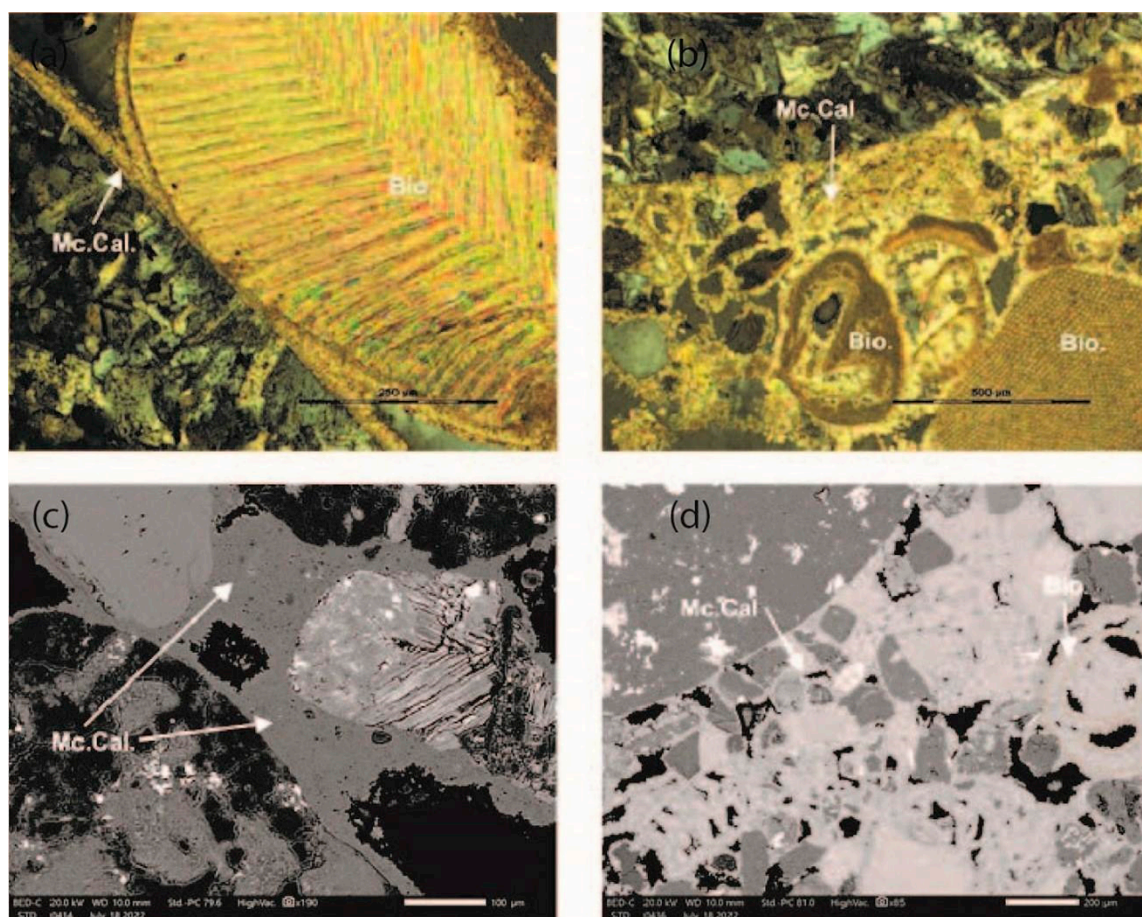


**Figure 10.** Xylophagou sample analysis; abbreviations: Mc.Cal., micritic High Magnesium Calcite. Polarised microscopy images (a) sample PV7, 20× magnification, scale 250 μm. Micritic HMC isopachous cement coating lithoclast and bioclast grains. (b) Sample PV15, 10× magnification, scale 500 μm. Micritic HMC cement is coating minerals, and lithoclast and bioclast grains. SEM images (c) sample PV7, scale 100 μm. The micritic HMC cement covers the sediment grains and fills the pores. (d) Sample PV15, scale 200 μm. Thin micritic HMC cement covering sediment grains; a notable number of bioclasts are observed.

Through the integration of microscopic analysis and a comprehensive field survey, we have substantiated that all the examined samples are indeed beachrock samples featuring intertidal cement. Consequently, the identified formation zone for the samples selected for OSL dating was the intertidal zone.

### 5.3. Mineralogy

The results of XRD data processing show that there were several similarities in the mineral composition of each sample of beachrock. The minerals contained in each of the six samples that have been analysed are composed mainly of silica, Calcite, Manganocalcite, Clinocllore, Magnesiohornblende, Clinopyroxene, and Albite (Table 1). All of these minerals are directly associated with the main geology of the island which is expressed by the Troodos terrain and the Circum Troodos sedimentary succession [67,68].

### 5.4. Relative Sea Level Calculations

All the samples collected from the beachrock were used as SLIPs. Every index point has a distinct vertical uncertainty that is determined by the measurement's precision as well as a number of variables related to the sample processing and collection [18].



Samples PL37 and PL30 from Pyla were collected from  $-0.22$  m and  $-0.19$  m, respectively. The OSL method provided ages of 0.36 ka for PL37 and 0.66 ka for sample PL30. Samples from the Paphos airport site (PA31 and PA17) provided ages of 1.0 ka and 1.26 ka and were collected from  $-0.18$  m and  $0.02$  m, respectively. The sample collected from Amathous (AM26), provided an age of 2.79 ka, and it was collected from a depth of  $-1.01$  m. The samples collected from Xylophagou (PV7 and PV15) provided ages of 2.17 ka and 71.1 ka and were located at 0.36 m amsl and  $-0.43$  m. The sample, PV15, provided an age which is not representative of the beachrock formation, and it is concluded that it was a fragment of the overlaying coastal conglomerate which was incorporated into the beachrock during its formation. All the details of the conversion to SLIP and calculations of the former relative sea level can be found in Tables 2 and 3.

**Table 2.** Mineral content and textural characteristics of beachrock derived from the microscopical analysis and association with SLIP and indicative meaning.

Sample	Cement Type	Cement Thickness	SLIP	Indicative Meaning
PA17	Thin isopachous micritic HMC. No matrix and no bioclasts	$<10\ \mu\text{m}$	Intertidal, undifferentiated	MHW to MLW
PA31	Thin isopachous bladed micritic HMC, brown coloured	$<8\ \mu\text{m}$	Intertidal, undifferentiated	MHW to MLW
AM1	Micritic HMC as pore filling. Brown-coloured well-developed crystals	$20\ \mu\text{m}$	Intertidal, undifferentiated	MHW to MLW
AM26	Isopachous micritic HMC as pore filling, meniscus, brown coloured. 10% bioclast contribution	$50\text{--}100\ \mu\text{m}$	Intertidal, undifferentiated	MHW to MLW
PL30	Bladed isopachous micritic HMC, brown coloured.	$10\text{--}20\ \mu\text{m}$	Intertidal, undifferentiated	MHW to MLW
PL37	Bladed isopachous micritic HMC, matrix infilling and pellet concentrations	$10\text{--}20\ \mu\text{m}$	Intertidal, undifferentiated	MHW to MLW
PV7	Isopachous micritic HMC, brown bio-micritic cement. Pellet concentrations	$10\text{--}20\ \mu\text{m}$	Intertidal, undifferentiated	MHW to MLW
PV15	Isopachous bladed micritic and sparitic HMC. 20% bioclast contribution	$\approx 40\ \mu\text{m}$	Not qualified	-----

**Table 3.** Relative sea level calculations. Uplift rates in this table were adopted by [58].

Beachrock ID	Height (m)	Age (ka)	Tidal Range (m)	Measurement Error (m)	Indicative Meaning (m)	RWL (m)	RSL (m)	Error (cm)	Uplift (mm/y)	Total Uplift Per Site (mm)	SL (m)
PL37	$-0.22$	0.36	0.41	0.05	0.42	0.21	$-0.43$	0.13	0.11	39.6	$-0.4696$
PL30	$-0.19$	0.66	0.41	0.05	0.42	0.21	$-0.4$	0.13	0.11	72.6	$-0.4726$
PA31	$-0.18$	1.03	0.41	0.05	0.42	0.21	$-0.39$	0.13	0.35	360.5	$-0.7505$
PA17	0.02	1.26	0.41	0.05	0.42	0.21	$-0.19$	0.13	0.35	441	$-0.631$
PV7	0.36	2.18	0.41	0.05	0.42	0.21	0.15	0.13	0.1	218	0.068
AM26	$-1.01$	2.79	0.41	0.05	0.42	0.21	$-1.22$	0.13	0.15	418.5	$-1.6385$

## 6. Discussion

The Holocene RSL fluctuations in the eastern Mediterranean have been subjected to significant scientific interest due to their implications for understanding regional climate dynamics, tectonic activity, and human development. [69] elaborated the predictions for the history of relative sea level at Lambousa (North coast of Cyprus) for the past 3.5 kyr, according to GIA models ICE-6G (VM5a) [70,71], ICE-7G (VM7) [72,73], and the GIA model by [74] (ANU), 2005 (Figure 11).

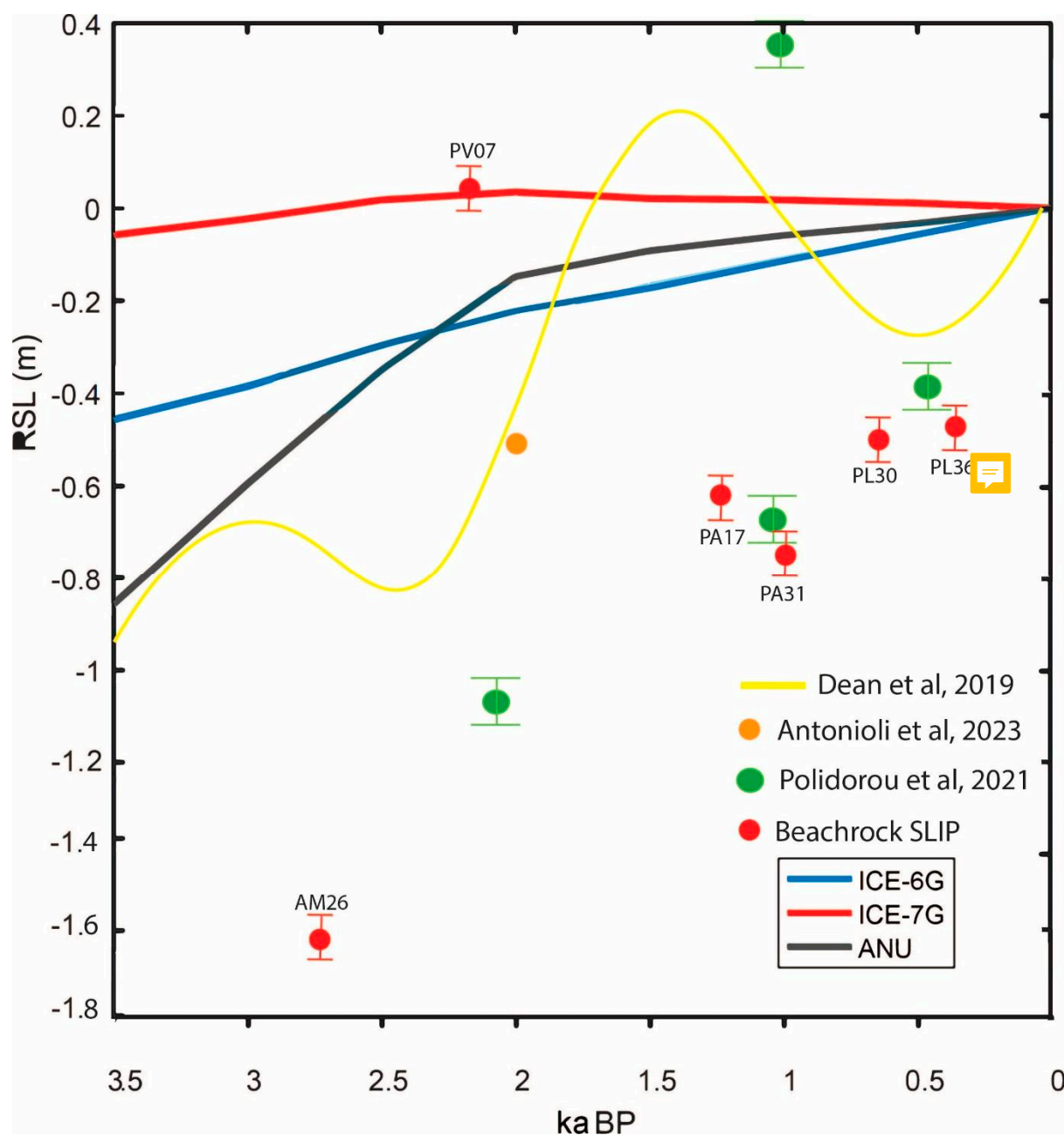


**Figure 11.** Relative sea-level change according to GIA models ICE-6G, ICE-7G, ANU [69] and sea-level curve for Israeli coast [18] (yellow line). Relative sea-level points (red circles) calculated in this study are based on beachrock SLIP. Orange circle symbol represents RSL point calculated by reference to archaeological indicator (Lambousa Fish Tank) [69], green circle symbols represent the RSL points calculated using beachrock at Akrotiri peninsula [11].

The RSL curve calculated in this study demonstrates a rise in the relative sea level from 3 ka up to 2.2 ka, where it reaches the present level. This agrees with the estimation of the ICE-7G model, and furthermore, it is in a good agreement with the estimations of a climatic warm episode in the Mediterranean which caused the rising in the RSL (Roman warm episode) [75,76]. From 2.2 ka up to 0.9 ka, a stable decrease in the RSL to  $-0.7$  m is observed which is in agreement with the general trend of the ICE-7G, and it is in close agreement with the period of regional cooling (13th century–18th century BCE), particularly to the North Atlantic region described by some authors as the Little Ice Age [77,78]. Curves ICE-6G and ANU predict a stable low rate in relative sea-level rise. From 0.9 ka to the present day, there is a gradual rising in the RSL up to the present level which agrees with

the Curves ICE-6G and ANU. Curve ICE-7G predicts a very slow decrease in the RSL to the current level.

Dean et al. (2019) [18] detected centennial-scale sea-level variations over the last three millennia by analysing coastal archaeological sites in Israel, specifically structures that are sensitive to sea-level changes, such as ancient harbours, fish ponds, and coastal fortifications. It was concluded that it is possible to detect centennial sea-level variations using archaeological evidence. The analysis showed distinct phases of sea-level rise and fall over the past 3000 years, including periods of relative stability followed by more rapid changes. The identified periods of sea-level rise corresponded with known climate changes (e.g., the Roman Warm Period and the Medieval Climate Anomaly) and sea-level fall during cooler periods (e.g., the Little Ice Age). The data from the coast of Israel follow the same trend of RSL oscillations as in this study

Previous attempts at the estimation of the RSL curve in the upper Holocene with the use of geomorphological features (beachrock) in Cyprus provided interesting results but they were limited to a local scale. Polidorou et al. (2021) [11] studied the beachrock formations of the Akrotiri Peninsula, southern Cyprus. The estimations of the relative sea level in the Akrotiri Peninsula at  $-1.15 \pm 0.13$  m at  $\sim 2150$  years BP, a rise of  $-0.7 \pm 0.13$  m at  $\sim 1150$  years BP, a rapid rise of  $0.42 \pm 0.13$  m at  $\sim 770$  years BP and a significant fall of  $-0.41 \pm 0.13$  m at 480 years BP before returning to present levels, are in close alignment with the results of this study, and they pinpoint the same trend in the oscillations of the relative sea level. The observed differences are probably due to the localised tectonic forces.

Other RSL change studies, based on archaeological evidence whose focus has been the south coast of the island [15,60,79], point towards different estimations, since they have been based on different proxies (i.e., tectonics, biological indicators). For this reason, the proposed RSL curve should be considered only as a first step towards the systematic documentation of the relative sea-level changes along the south coast. In the future, it can be further augmented by using other proxies to enhance the precision.

Nevertheless, based on this RSL curve, it is possible to correlate the changes with the archaeological and historical context of the island. During the Classical and Hellenistic periods, RSL was not very different from that of today. These periods coincided with the construction of the first artificial harbours [53] on the island. This interestingly may indicate the fact that the Classical harbour structures are submerged today (i.e., Amathous, Akrotiri-Dreamer's Bay, Kourion) mainly due to the loss of the upper courses of the ashlar-built structures, and other local geological phenomena (i.e., liquefaction, subsidence, tectonic activity) rather than the change in RSL. Finally, the low sea level at the end of the Roman period and during the Byzantine period corresponds to the situation attested to at Amathous. This RSL estimation calls for attention to conduct further research on a subject that has been relatively neglected, that of Byzantine and Medieval coastal remains.

## 7. Conclusions

This relative sea-level change curve for the south coast of Cyprus indicates that in the Classical period, the RSL corresponded to today's sea level. It gradually declined till the Roman period and continued to decrease in the Byzantine times. It is important to note that this pattern cannot be applied to all sites due to the different dynamics that form the coastline (i.e., sediment input, tectonics), but it is a starting point that will contribute to the study, and the interpretation of coastal sites as well as the identification of areas of archaeological interest that have not yet been under study. Also, further work to enrich this RSL curve will considerably contribute to greater accuracy and detail not only for future archaeological research but also for the management, safeguarding, and protection of coastal heritage.

The beachrock dates also offer an opportunity for future assessment. The Xylofagou beachrock (PV7) dates to the Hellenistic Period (230 BCE), the Paphos Airport samples (PA17 and PA31) were dated to the Byzantine period (690 CE and 920 CE), and the Pyla beachrock (PL30, PL37) indicates a paleoshoreline dating to the Medieval period (1290 CE and 1590 CE). These once correlated with the nearby archaeological remains, and additional geological data could provide further input on the changes in the coastline at the specific sites. Such potential is visible in the Amathous (AMS26) sample which is located at  $-1.00$  m below the current sea level and is located at 65 m from the current coastline, in the submerged Hellenistic harbour basin. Its date of 2790 BP corresponds to the Cypro-Geometric period (around 1100–750 BCE). From this beachrock sample, a possible paleo-coastline can be reconstructed for the Cypro-Geometric period for the first time. The location and dating of this beachrock along with the rich archaeological documentation in the area [66] indicate the potential and need for further geoarchaeological investigation in the area.

Beachrock formations can serve as reliable indicators of past RSLs and coastal dynamics. Combining dating techniques with geological analysis offers insights into the evolution of the region over the Holocene, contributing to our understanding of Mediterranean coastal changes. The results of this study help improve the data of long-term sea-level variability in the eastern Mediterranean, contributing to broader research on regional climate and sea-level responses.

Furthermore, this research can provide a connection between the archaeological research with climate science, providing an insight into how ancient societies interacted with the changing coastal environments.

**Author Contributions:** Conceptualisation, M.P.; investigation, M.P., G.S. and J.G.; methodology, G.S. and A.K.; supervision, M.P.; validation, M.P. and A.K.; writing—original draft, M.P.; writing—review and editing, G.S., A.K. and J.G. All authors have read and agreed to the published version of the manuscript.

**Funding:** This research was funded by Honor Frost Foundation, 10 Carlton House Terrace, London SW1Y 5AH, “Big Grant Award”.

**Data Availability Statement:** The data are available through the Honor Frost Foundation website: <https://honorfrostfoundation.org/> (accessed on 6 April 2024).

**Conflicts of Interest:** The authors declare no conflicts of interest.

## References

1. Bar, A.; Bookman, R.; Galili, E.; Zviely, D. Beachrock Morphology along the Mediterranean Coast of Israel: Typological Classification of Erosion Features. *J. Mar. Sci. Eng.* **2022**, *10*, 1571. [CrossRef]
2. Falkenroth, M.; Schneider, B.; Hoffmann, G. Beachrock as Sea-Level Indicator e A Case Study at the Coastline of Oman (Indian Ocean). *Quat. Sci. Rev.* **2019**, *206*, 81–98. [CrossRef]
3. Romine, B.M.; Fletcher, C.H.; Frazer, L.N.; Anderson, T.R. Beach Erosion under Rising Sea-Level Modulated by Coastal Geomorphology and Sediment Availability on Carbonate Reef-Fringed Island Coasts. *Sedimentology* **2016**, *63*, 1321–1332. [CrossRef]
4. Danjo, T.; Kawasaki, S. Characteristics of Beachrocks: A Review. *Geotech. Geol. Eng.* **2014**, *32*, 215–246. [CrossRef]
5. Giresse, P.; Berné, S.; Certain, R.; Courp, T.; Hebert, B.; Raynal, O. Beachrocks and Lithified Barriers in the Gulf of Lions (Western Mediterranean Sea) as New Markers of the Last Sea-Level Rise. *Sedimentology* **2023**, *70*, 569–591. [CrossRef]
6. Mastronuzzi, G.; De Giosa, F.; Quarta, G.; Pallara, M.; Scardino, G.; Scicchitano, G.; Peluso, C.; Antropoli, C.; Caporale, C.; Demarte, M. Holocene Sea Level Recorded by Beach Rocks at Ionian Coasts of Apulia (Italy). *Geosciences* **2023**, *13*, 194. [CrossRef]
7. Smith, C.G.; Jones, M.C.; Osterman, L.E.; Passeri, D.L. Using Multiple Environmental Proxies and Hydrodynamic Modeling to Investigate Late Holocene Climate and Coastal Change within a Large Gulf of Mexico Estuarine System (Mobile Bay, Alabama, USA). *Mar. Geol.* **2020**, *427*, 106218. [CrossRef]
8. Bar-Yosef Mayer, D.E.; Kahanov, Y.; Roskin, J.; Gildor, H. Neolithic Voyages to Cyprus: Wind Patterns, Routes, and Mechanisms. *J. Isl. Coast. Archaeol.* **2015**, *10*, 412–435. [CrossRef]



9. Devillers, B.; Brown, M.; Morhange, C. Paleo-Environmental Evolution of the Larnaca Salt Lakes (Cyprus) and the Relationship to Second Millennium BC Settlement. *J. Archaeol. Sci. Rep.* **2015**, *1*, 73–80. [\[CrossRef\]](#)
10. Morhange, C.; Goiran, J.P.; Bourcier, M.; Carbonel, P.; Le Campion, J.; Rouchy, J.M.; Yon, M. Recent Holocene Paleo-Environmental Evolution and Coastline Changes of Kition, Larnaca, Cyprus, Mediterranean Sea. *Mar. Geol.* **2000**, *170*, 205–230. [\[CrossRef\]](#)
11. Polidorou, M.; Saitis, G.; Evelpidou, N. Beachrock Development as an Indicator of Paleogeographic Evolution, the Case of Akrotiri Peninsula, Cyprus. *Z. Für Geomorphol.* **2021**, *63*, 3–17. [\[CrossRef\]](#)
12. Mohapatra, P.P.; Stephen, A.; Singh, P.; Prasad, S.; Anupama, K. Pollen Based Inference of Holocene Sea Level Changes, Depositional Environment and Climatic History of Cauvery Delta, Southern India. *Catena* **2021**, *199*, 105029. [\[CrossRef\]](#)
13. Wang, S.; Li, Y.; Fan, B.; Cao, Y.; You, H.; Wang, R.; Ge, Y.; Da, S.; She, Z.; Zhang, Z.; et al. Middle to Late Holocene Environmental Evolution and Sea Level Change on the West Coast of Bohai Bay. *Quat. Int.* **2023**, *669*, 20–31. [\[CrossRef\]](#)
14. Yang, D.-Y.; Han, M.; Yoon, H.H.; Kim, J.C.; Choi, E.; Shin, W.-J.; Kim, J.-Y.; Jung, A.; Park, C.; Jun, C.-P. Holocene Relative Sea-Level Changes on the Southern East Coast of the Yellow Sea Holocene Relative Sea-Level Change GIA Model Levering Effect. *Palaeogeogr. Palaeoclim. Palaeoecol.* **2023**, *629*, 111779. [\[CrossRef\]](#)
15. Galili, E.; Şevketoğlu, M.; Salamon, A.; Zviely, D.; Mienis, H.K.; Rosen, B.; Moshkovitz, S. Late Quaternary Beach Deposits and Archaeological Relicts on the Coasts of Cyprus, and the Possible Implications of Sea-Level Changes and Tectonics on the Early Populations. *Geol. Soc. Spec. Publ.* **2016**, *411*, 179–218. [\[CrossRef\]](#)
16. Mattei, G.; Vacchi, M. The Geographic Variability of the Millennial Sea-Level Changes along the Coasts of Italy. *Alp. Mediterr. Quat.* **2023**, *36*, 63–74. [\[CrossRef\]](#)
17. Vacchi, M.; Ghilardi, M.; Melis, R.T.; Spada, G.; Giaime, M.; Marriner, N.; Lorscheid, T.; Morhange, C.; Burjachs, F.; Rovere, A. New Relative Sea-Level Insights into the Isostatic History of the Western Mediterranean. *Quat. Sci. Rev.* **2018**, *201*, 396–408. [\[CrossRef\]](#)
18. Dean, S.; Horton, B.P.; Evelpidou, N.; Cahill, N.; Spada, G. Can We Detect Centennial Sea-Level Variations over the Last Three Thousand Years in Israeli Archaeological Records? *Quat. Sci. Rev.* **2019**, *210*, 125–135. [\[CrossRef\]](#)
19. Karkani, A.; Evelpidou, N.; Giaime, M.; Marriner, N.; Morhange, C.; Spada, G. Late Holocene Sea-Level Evolution of Paros Island (Cyclades, Greece). *Quat. Int.* **2019**, *500*, 139–146. [\[CrossRef\]](#)
20. Evelpidou, N.; Kampilis, I.; Pirazzoli, P.A.; Vassilopoulos, A. Global Sea-Level Rise and the Disappearance of Tidal Notches. *Glob. Planet. Change* **2012**, *92–93*, 248–256. [\[CrossRef\]](#)
21. Sivan, D.; Wdowinski, S.; Lambeck, K.; Galili, E.; Raban, A. Holocene Sea-Level Changes along the Mediterranean Coast of Israel, Based on Archaeological Observations and Numerical Model. *Palaeogeogr. Palaeoclim. Palaeoecol.* **2001**, *167*, 101–117. [\[CrossRef\]](#)
22. Pirazzoli, P.A.; Thommeret, J.; Thommeret, Y.; Laborel, J.; Montag-Gioni, L.F. Crustal Block Movements from Holocene Shorelines: Crete and Antikythera (Greece). *Tectonophysics* **1982**, *86*, 27–43. [\[CrossRef\]](#)
23. Antonioli, F.; De Falco, G.; Presti, V.L.; Moretti, L.; Scardino, G.; Anzidei, M.; Bonaldo, D.; Carniel, S.; Leoni, G.; Furlani, S.; et al. Relative Sea-Level Rise and Potential Submersion Risk for 2100 on 16 Coastal Plains of the Mediterranean Sea. *Water* **2020**, *12*, 2173. [\[CrossRef\]](#)
24. Danezis, C.; Nikolaidis, M.; Mettas, C.; Hadjimitsis, D.G.; Kokosis, G.; Kleanthous, C. Establishing an Integrated Permanent Sea-Level Monitoring Infrastructure towards the Implementation of Maritime Spatial Planning in Cyprus. *J. Mar. Sci. Eng.* **2020**, *8*, 861. [\[CrossRef\]](#)
25. Monioudi, I.N.; Velegrakis, A.F.; Chatzistratis, D.; Voutsoukas, M.I.; Savva, C.; Wang, D.; Bove, G.; Mentaschi, L.; Paprotny, D.; Morales-Ná Poles, O.; et al. Climate Change-Induced Hazards on Touristic Island Beaches: Cyprus, Eastern Mediterranean. *Front. Mar. Sci.* **2023**, *10*, 1188896. [\[CrossRef\]](#)
26. Saitis, G.; Karkani, A.; Evelpidou, N.; Maroukian, H. Palaeogeographical Reconstruction of Ancient Diolkos Slipway by Using Beachrocks as Proxies, West Corinth Isthmus, Greece. *Quaternary* **2022**, *5*, 7. [\[CrossRef\]](#)
27. Ozturk, M.Z.; Erginal, A.E.; Kiyak, N.G.; Ozturk, T. Cement Fabrics and Optical Luminescence Ages of Beachrock, North Cyprus: Implications for Holocene Sea-Level Changes. *Quat. Int.* **2016**, *401*, 132–140. [\[CrossRef\]](#)
28. Karkani, A.; Evelpidou, N.; Vacchi, M.; Morhange, C.; Tsukamoto, S.; Frechen, M.; Maroukian, H. Tracking Shoreline Evolution in Central Cyclades (Greece) Using Beachrocks. *Mar. Geol.* **2017**, *388*, 25–37. [\[CrossRef\]](#)
29. Mauz, B.; Vacchi, M.; Green, A.; Hoffmann, G.; Cooper, A. Beachrock: A Tool for Reconstructing Relative Sea Level in the Far-Field. *Mar. Geol.* **2015**, *362*, 1–16. [\[CrossRef\]](#)
30. Poole, A.J.; Robertson, A.H.F. Quaternary Uplift and Sea-Level Change at an Active Plate Boundary, Cyprus. *J. Geol. Soc. Lond.* **1991**, *148*, 909–921. [\[CrossRef\]](#)
31. Poole, A.J.; Robertson, A.; Panayides, I.; Xenophontos, C.; Malpas, J. Quaternary Marine Terraces and Aeolianites in Coastal South and West Cyprus: Implications for Regional Uplift and Sea-Level Change. In Proceedings of the Third International Conference on the Geology of the Eastern Mediterranean, Nicosia, Cyprus, 23–26 September 1998; proceedings 2000. pp. 105–123.
32. Waters, J.V.; Jones, S.J.; Armstrong, H.A. Climatic Controls on Late Pleistocene Alluvial Fans, Cyprus. *Geomorphology* **2010**, *115*, 228–251. [\[CrossRef\]](#)

33. Massari, F.; Capraro, L.; Rio, D. Climatic Modulation of Timing of Sytems-Tract Development with Respect to Sea-Level Changes (Middle Pleistocene of Crotona, Calabria, Southern Italy). *J. Sediment. Res.* **2007**, *77*, 461–468. [\[CrossRef\]](#)
34. Quigley, M.C.; Sandiford, M.; Cupper, M.L. Distinguishing Tectonic from Climatic Controls on Range-Front Sedimentation. *Basin Res.* **2007**, *19*, 491–505. [\[CrossRef\]](#)
35. Lambeck, K.; Esat, T.M.; Potter, E.K. Links between Climate and Sea Levels for the Past Three Million Years. *Nature* **2002**, *419*, 199–206. [\[CrossRef\]](#) [\[PubMed\]](#)
36. Le Pichon, X.; Kreemer, C. The miocene-to-present kinematic evolution of the eastern mediterranean and middle east and its implications for dynamics. *Annu. Rev. Earth Planet. Sci.* **2010**, *38*, 323–351. [\[CrossRef\]](#)
37. Aksu, A.E.; Hall, J.; Yaltirak, C. Miocene to Recent tectonic evolution of the eastern Mediterranean: New pieces of the old Mediterranean puzzle. *Mar. Geol.* **2005**, *221*, 1–13. [\[CrossRef\]](#)
38. Kempler, D.; Garfunkel, Z. Structures and kinematics in the northeastern Mediterranean: A study of an irregular plate boundary. *Tectonophysics* **1994**, *234*, 19–32. [\[CrossRef\]](#)
39. Brew, G.; Barazangi, M.; Al-Maleh, A.K.; Sawaf, T. Tectonic and Geologic Evolution of Syria. *GeoArabia* **2001**, *6*, 573–616.
40. Montadert, L.; Nicolaides, S.; Semb, H.P. Lie Petroleum systems offshore Cyprus. In *Petroleum Systems of the Tethyan Region*; Marlow, L., Kendall, C., Yose, L., Eds.; AAPG Memoir: Tulsa, OK, USA, 2014; Volume 106, pp. 301–334.
41. Bowman, S.A. Regional seismic interpretation of the hydrocarbon prospectivity of offshore Syria. *GeoArabia* **2011**, *16*, 95–124.
42. Faccenna, C.; Bellier, O.; Martinod, J.; Piromallo, C.; Regard, V. Slab detachment beneath eastern Anatolia: A possible cause for the formation of the North Anatolian fault. *Earth Planet. Sci. Lett.* **2006**, *242*, 85–97. [\[CrossRef\]](#)
43. Robertson, A.H.F.; Parlak, O.; Ustaömer, T. Overview of the Palaeozoic–Neogene evolution of Neotethys in the Eastern Mediterranean region (southern Turkey, Cyprus, Syria). *Pet. Geosci.* **2012**, *18*, 381–404. [\[CrossRef\]](#)
44. McClusky, S.; Balassanian, S.; Barka, A.; Demir, C.; Ergintav, S.; Georgiev, I.; Gurkan, O.; Hamburger, M.; Hurst, K.; Kahle, H.; et al. Global Positioning System constraints on plate kinematics and dynamics in the eastern Mediterranean and Caucasus. *J. Geophys. Res.* **2000**, *105*, 5695–5719. [\[CrossRef\]](#)
45. Reilinger, R.; McClusky, S.; Vernant, P.; Lawrence, S.; Ergintav, S.; Cakmak, R.; Ozener, H.; Kadirov, F.; Guliev, I.; Stepanyan, R. GPS constraints on continental deformation in the Africa-Arabia-Eurasia continental collision zone and implications for the dynamics of plate interactions. *J. Geophys. Res.* **2006**, *111*, B05411. [\[CrossRef\]](#)
46. Vidal, N.; Alvarez-Marrón, J.; Klaeschen, D. The structure of the Africa-Anatolia plate boundary in the eastern Mediterranean. *Tectonics* **2000**, *19*, 723–739. [\[CrossRef\]](#)
47. Simmons, A.H. Whose Myth? Archaeological Data, Interpretations, and Implications for the Human Association with Extinct Pleistocene Fauna at Akrotiri Aetokremnos, Cyprus. *J. Mediterr. Archaeol.* **1996**, *9*, 97–105. [\[CrossRef\]](#)
48. Mandel, R.D.; Simmons, A.H. Akrotiri Aetokremnos, Cyprus. In *Encyclopedia of Geoarchaeology*; Gilbert, A.S., Ed.; Encyclopedia of Earth Sciences Series; Springer: Dordrecht, The Netherlands, 2017. [\[CrossRef\]](#)
49. Blackwell, N.G. The Archaeology of Cyprus: From Earliest Prehistory through the Bronze Age. By A. Bernard Knapp. New York: Cambridge University Press, 2013. Pp. xx + 640 + 152 Figures + 5 Tables. \$38.99 (Paperback). *J. Near East. Stud.* **2015**, *74*, 162–165. [\[CrossRef\]](#)
50. Keswani, P.S.; Keswani, P.S. Hierarchies, Heterarchies, and Urbanization Processes: The View from Bronze Age Cyprus. *J. Mediterr. Archaeol.* **1997**, *9*, 211–250. [\[CrossRef\]](#)
51. Iacovou, M. The Early Iron Age Urban Forms of Cyprus, in Mediterranean Urbanization 800–600 B.C. In *Proceedings of the British Academy* 126; Osborne, R., Cunliffe, B., Eds.; Oxford University Press: Oxford, UK, 2005; pp. 17–43. Available online: [https://www.academia.edu/4152489/\\_Iacovou\\_M\\_2005\\_The\\_Early\\_Iron\\_Age\\_Urban\\_Forms\\_of\\_Cyprus\\_in\\_Mediterranean\\_Urbanization\\_800\\_600\\_B\\_C\\_Robin\\_Osborne\\_and\\_Barry\\_Cunliffe\\_eds\\_Proceedings\\_of\\_the\\_British\\_Academy\\_126\\_Oxford\\_University\\_Press\\_17\\_43](https://www.academia.edu/4152489/_Iacovou_M_2005_The_Early_Iron_Age_Urban_Forms_of_Cyprus_in_Mediterranean_Urbanization_800_600_B_C_Robin_Osborne_and_Barry_Cunliffe_eds_Proceedings_of_the_British_Academy_126_Oxford_University_Press_17_43) (accessed on 6 March 2024).
52. Iacovou, M. From the Late Cypriot Polities to the Iron Age “Kingdoms”: Understanding the Political Landscape of Cyprus from Within. *Les. Roy. Chypr À L’épreuve L’histoire* **2018**, *60*, 7–28. [\[CrossRef\]](#)
53. Theodoulou, T. Ναυτική Δραστηριότητα Και Λιμενικό Δίκτυο Στην Κλασική Κύπρο. Ph.D. Thesis, University of Cyprus, Nicosia, Cyprus, 2007. Available online: <https://www.ancientportsantiques.com/wp-content/uploads/Documents/PLACES/Crete-Cyprus/Cyprus-TheodoulouPhD2007.pdf> (accessed on 5 February 2024).
54. Satraki, A. Abnormal Functional Activation and Maturation of Fronto-Striato-Temporal and Cerebellar Regions During Sustained Attention in Autism Spectrum Disorder. *Am. J. Psychiatry* **2010**, *171*, 1107–1116. [\[CrossRef\]](#)
55. Bekker-Nielsen, T. *The Roads of Ancient Cyprus*; Museum Tusculanum Press: Copenhagen, Denmark, 2004.
56. Leidwanger, J. Opportunistic Ports and Spaces of Exchange in Late Roman Cyprus. *J. Marit. Archaeol.* **2013**, *8*, 221–243. [\[CrossRef\]](#)
57. Panayides, P.; Jacobs, I. *Cyprus in the Long Late Antiquity. History and Archaeology Between the Sixth and Eighth Centuries*; Oxbow Books: Oxford, UK, 2023.
58. Demesticha, S. Cutting a Long Story Short? Underwater and Maritime Archaeology in Cyprus. *J. East. Mediterr. Archaeol. Herit. Stud.* **2018**, *6*, 62–78. [\[CrossRef\]](#)

59. Leonard, J.R. American Archaeologists in Cypriot Waters: One Nation's Contributions to the Underwater Exploration of Cyprus' Past. *Near East. Archaeol.* **2008**, *71*, 130–138. [\[CrossRef\]](#)
60. Callot, O.; Fourrier, S.; Yon, M. Kition-Bamboula VIII: Le Port de Guerre de Kition. In *Kition-Bamboula VIII*; MOM Editions: Lyon, France, 2022. [\[CrossRef\]](#)
61. Moska, P.; Bluszcz, A.; Poreba, G.; Tudyka, K.; Adamiec, G.; Szymak, A.; Przybyła, A. Luminescence Dating Procedures at the Gliwice Luminescence Dating Laboratory. *Geochronometria* **2021**, *48*, 1–15. [\[CrossRef\]](#)
62. Hijma, M.P.; Engelhart, S.E.; Törnqvist, T.E.; Horton, B.P.; Hu, P.; Hill, D.F. A protocol for a geological sea-level database. In *Handbook of Sea-Level Research*; Shennan, I., Long, A.J., Horton, B.P., Eds.; Wiley: Hoboken, NJ, USA, 2015. [\[CrossRef\]](#)
63. Khan, M.N.H.; Danjo, T.; Kawasaki, S. Artificial Beachrock Formation through Sand Solidification towards the Inhibit of Coastal Erosion in Bangladesh. *Int. J. Geomate* **2015**, *9*, 1528–1533. [\[CrossRef\]](#)
64. Vacchi, M.; Marriner, N.; Morhange, C.; Spada, G.; Fontana, A.; Rovere, A. Earth-Science Reviews Multiproxy Assessment of Holocene Relative Sea-Level Changes in the Western Mediterranean: Sea-Level Variability and Improvements in the de Fi Nition of the Isostatic Signal. *Earth Sci. Rev.* **2016**, *155*, 172–197. [\[CrossRef\]](#)
65. Mattei, G.; Caporizzo, C.; Corrado, G.; Vacchi, M.; Stocchi, P.; Pappone, G.; Schiattarella, M.; Aucelli, P.P.C. On the Influence of Vertical Ground Movements on Late-Quaternary Sea-Level Records. A Comprehensive Assessment along the Mid-Tyrrhenian Coast of Italy (Mediterranean Sea). *Quat. Sci. Rev.* **2022**, *279*, 107384. [\[CrossRef\]](#)
66. Empereur, J.-Y.; Koželj, T.; Picard, O.; Wurch-Koželj, M. *The Hellenistic Harbour of Amathus. Underwater Excavations, 1984–1986. Volume 1: Architecture and History*; Peeters Publishers: Leuven, Belgium, 2017. [\[CrossRef\]](#)
67. Kinnaird, T.C.; Robertson, A.H.F.; Morris, A. Timing of Uplift of the Troodos Massif (Cyprus) Constrained by Sedimentary and Magnetic Polarity Evidence. *J. Geol. Soc. Lond.* **2011**, *168*, 457–470. [\[CrossRef\]](#)
68. Ring, U.; Pantazides, H. The Uplift of the Troodos Massif, Cyprus. *Tectonics* **2019**, *38*, 3124–3139. [\[CrossRef\]](#)
69. Antonioli, F.; Furlani, S.; Spada, G.; Melini, D.; Zomeni, Z. The Lambousa (Cyprus) Fishtank in a Quasi-Stable Coastal Area of the Eastern Mediterranean, a Notable Marker for Testing GIA Models. *Geosciences* **2023**, *13*, 280. [\[CrossRef\]](#)
70. Argus, D.F.; Peltier, W.R.; Drummond, R.; Moore, A.W. The Antarctica Component of Postglacial Rebound Model ICE-6G\_C (VM5a) Based on GPS Positioning, Exposure Age Dating of Ice Thicknesses, and Relative Sea Level Histories. *Geophys. J. Int.* **2014**, *198*, 537–563. [\[CrossRef\]](#)
71. Peltier, W.R.; Argus, D.F.; Drummond, R. Space Geodesy Constrains Ice Age Terminal Deglaciation: The Global ICE-6G\_C (VM5a) Model. *J. Geophys. Res. Solid. Earth* **2015**, *120*, 450–487. [\[CrossRef\]](#)
72. Roy, K.; Peltier, W.R. Space-Geodetic and Water Level Gauge Constraints on Continental Uplift and Tilting over North America: Regional Convergence of the ICE-6G\_C (VM5a/VM6) Models. *Geophys. J. Int.* **2017**, *210*, 1115–1142. [\[CrossRef\]](#)
73. Roy, K.; Peltier, W.R. Glacial Isostatic Adjustment, Relative Sea Level History and Mantle Viscosity: Reconciling Relative Sea Level Model Predictions for the U.S. East Coast with Geological Constraints. *Geophys. J. Int.* **2015**, *201*, 1156–1181. [\[CrossRef\]](#)
74. Lambeck, K.; Purcell, A. Sea-Level Change in the Mediterranean Sea since the LGM: Model Predictions for Tectonically Stable Areas. *Quat. Sci. Rev.* **2005**, *24*, 1969–1988. [\[CrossRef\]](#)
75. Erdkamp, P. *Climate Change and the Productive Landscape in the Mediterranean Region in the Roman Period*; Springer: Berlin/Heidelberg, Germany, 2021; pp. 411–442. [\[CrossRef\]](#)
76. Margaritelli, G.; Cacho, I.; Català, A.; Barra, M.; Bellucci, L.G.; Lubritto, C.; Rettori, R.; Lirer, F. Persistent Warm Mediterranean Surface Waters during the Roman Period. *Sci. Rep.* **2020**, *10*, 1–10. [\[CrossRef\]](#) [\[PubMed\]](#)
77. Lehmkuhl, F.; Owen, L. Late Quaternary Glaciation of Tibet and the Bordering Mountains: A Review. *Boreas* **2005**, *34*, 87–100. [\[CrossRef\]](#)
78. Winkler, S. Terminal Moraine Formation Processes and Geomorphology of Glacier Forelands at the Selected Outlet Glaciers of Jostedalbreen, South Norway. In *Landscapes and Landforms of Norway*; World Geomorphological Landscapes; Beylich, A.A., Ed.; Springer: Cham, Switzerland, 2021. [\[CrossRef\]](#)
79. Dalongeville, R.; Bernier, P.; Prieur, A.; Le Campion, T. Les Variations Récentes de La Ligne de Rivage Du Sud-Est de Chypre/The Early Changes of Southeastern Cyprus Shorelines. *Géomorphologie: Relief, processus, environnement. Geomorphology* **2000**, *6*, 13–19. [\[CrossRef\]](#)

**Disclaimer/Publisher's Note:** The statements, opinions and data contained in all publications are solely those of the individual author(s) and contributor(s) and not of MDPI and/or the editor(s). MDPI and/or the editor(s) disclaim responsibility for any injury to people or property resulting from any ideas, methods, instructions or products referred to in the content.